Spontaneous changes in brain striatal dopamine synthesis and storage dynamics *ex vivo* reveal end-product feedback-inhibition of tyrosine hydroxylase

Marta González-Sepúlveda [a,b,f], Muhammad Yusof Omar [a,b], Sally Hamdon [a,b], Guofen Ma [a,b], Santi Rosell-Vilar [a], Noora Raivio [a], Doaa Abass [a], Anna Martínez-Rivas [a,b], Miquel Vila [a,f,g], Jesús Giraldo [a,c,e], Montserrat Carrascal [d], Joaquín Abián [d], Carles Gil [a,b,1], Josefa Sabriá [a,b,1], Jordi Ortiz [a,b,e,*,1], David Moreno-Delgado [a,b,1]

[a] *Neuroscience Institute, School of Medicine, Universitat Autònoma de Barcelona, Spain*
[b] *Department of Biochemistry and Molecular Biology, Universitat Autònoma de Barcelona, Spain*
[c] *Biostatistics Unit, Universitat Autònoma de Barcelona, Spain*
[d] *Biological and Environmental Proteomics, IIBB-CSIC/IDIBAPS, Barcelona, Spain*
[e] *Centro Investigación Biomédica en Red de Salud Mental, CIBERSAM, and Translational Neuroscience Unit, Parc Taulí University Hospital and Universitat Autònoma de Barcelona, Spain*
[f] *Neurodegenerative Diseases Research Group, Vall d'Hebron Research Institute (VHIR)-Network Center for Biomedical Research in Neurodegenerative Diseases (CIBERNED), Spain*
[g] *Catalan Institution for Research and Advanced Studies (ICREA), Spain*

ARTICLE INFO

ABSTRACT

Synaptic events are important to define treatment strategies for brain disorders. In the present paper, freshly obtained rat brain striatal minces were incubated under different times and conditions to determine dopamine biosynthesis, storage, and tyrosine hydroxylase phosphorylation. Remarkably, we found that endogenous dopamine spontaneously accumulated during tissue incubation at 37 °C *ex vivo* while dopamine synthesis simultaneously decreased. We analyzed whether these changes in brain dopamine biosynthesis and storage were linked to dopamine feedback inhibition of its synthesis-limiting enzyme tyrosine hydroxylase. The aromatic-L-amino-acid decarboxylase inhibitor NSD-1015 prevented both effects. As expected, dopamine accumulation was increased with L-DOPA addition or VMAT2-overexpression, and dopamine synthesis decreased further with added dopamine, the VMAT2 inhibitor tetrabenazine or D_2 auto-receptor activation with quinpirole, accordingly to the known synaptic effects of these treatments. Phosphorylation activation and inhibition of tyrosine hydroxylase on Ser31 and Ser40 with okadaic acid, Sp-cAMP and PD98059 also exerted the expected effects. However, no clear-cut association was found between dopamine feedback inhibition of its own biosynthesis and changes of tyrosine hydroxylase phosphorylation, assessed by Western blot and mass spectrometry. The later technique also revealed a new Thr30 phosphorylation in rat tyrosine hydroxylase. Our methodological assessment of brain dopamine synthesis and storage dynamics *ex vivo* could be applied to predict the *in vivo* effects of pharmacological interventions in animal models of dopamine-related disorders.

1. Introduction

Excessive dopaminergic neurotransmission contributes to hyperkinetic movement disorders and psychotic episodes, and these conditions are currently treated with dopamine (DA)-interfering drugs. Because DA storage determines stimulus-dependent DA release, drugs

---

reducing DA storage by inhibiting VMAT2 transporters have become first-line treatments for Huntington's disease, tardive dyskinesia and Tourette syndrome (Jankovic, 2016). However, VMAT2 inhibition also produces very common side-effects that require medical attention, partly related to the fact that VMAT2 is not DA-selective, and therefore its inhibition reduces neurotransmission mediated by other monoamines. Catecholamine synthesis inhibition could -putatively- maintain the clinical benefits and avoid some unwanted effects of VMAT2 inhibition (Ankenman and Salvatore, 2007). For these reasons, an experimental model to simultaneously assess DA synthesis and storage under the influence of different combinations of drugs could be of interest.

Tyrosine hydroxylase (TH; tyrosine 3-monooxygenase; E.C. 1.14.16.2) is the first and rate-limiting enzyme in dopamine biosynthesis. Regulatory mechanisms of TH activity involve gene expression, phosphorylation and end-product feedback inhibition by catecholamines (Spector et al., 1967). The TH protein has been proposed to be a homotetramer where each monomer contains a phosphorylatable N-terminal domain that enhances cofactor affinity and enzymatic activity (Dunkley et al., 2004; Dunkley and Dickson, 2019; Haycock and Haycock, 1991; Lindgren et al., 2000; Zhang et al., 2014). TH phosphorylation has been extensively investigated, as changes in TH phosphorylation state are generally considered to be critical in the short-term regulation of DA biosynthesis (Haycock and Haycock, 1991). In particular, phosphorylations in Ser40, Ser31 and Ser19 of TH by several kinases including PKA, ERK and CaMKII enhance its enzymatic activity, thereby stimulating the synthesis of the neurotransmitter (Dunkley and Dickson, 2019; Harada et al., 1996; Lindgren et al., 2000). In addition, phosphorylation can also modulate TH action by stabilization of the protein (Nakashima et al., 2013) or affect TH binding to partners, such as 14-3-3 isoforms (Ghorbani et al., 2020). On the other hand, the mechanisms of end-product feedback inhibition are less clear. It is currently accepted that catecholamines bind to TH with high affinity (K_D 4 nM for DA) and that phosphorylation increases K_D for DA to 78–208 nM, relieving feedback inhibition (McCulloch et al., 2001; Ramsey and Fitzpatrick, 1998; Sura et al., 2004). *In vitro* studies using recombinant TH suggested that each TH dimer of the homotetramer could present a second DA binding site of low affinity (K_D 90 nM) (Briggs et al., 2011, 2014; Dickson and Briggs, 2013; Dunkley and Dickson, 2019; Gordon et al., 2008, 2009). This would imply simultaneous DA binding to high- and low-affinity sites inhibiting TH. However, these results could also be explained by distinct TH conformations in the homotetramer where a single DA binding site presents different K_D values in each monomer (Tekin et al., 2014).

Computational analysis have indicated the potential importance of feedback inhibition for dopaminergic neurotransmission (Justice et al., 1988; Wallace, 2007). Its experimental study is difficult due to the presence of indeterminate amounts of endogenous DA bound to TH *in vivo*. Furthermore, methods to estimate TH activity in brain usually block DA formation by inhibiting aromatic-L-amino-acid decarboxylase to accumulate L-DOPA (Lindgren et al., 2000), preventing to estimate DA feedback. To overcome this limitation, in this paper we modified the L-DOPA accumulation method and compared it to a radioisotopic method that accurately determines [³H]-DA synthesis from [³H]-tyrosine in rat striatal minces (Ma et al., 2014). By using both methods we were surprised to clearly observe that incubating brain tissue *ex vivo* at 37 °C was sufficient to induce an initially high DA synthesis and storage in vesicles. When storage approached saturation, end-product feedback inhibition of TH became the main factor limiting new DA biosynthesis.

2. Materials and methods

2.1. Chemicals

Opti-Phase HiSafe-3 liquid scintillation cocktail (Cat. No. 1200.437) and [3, 5-³H]-L-tyrosine (³H-Tyr, 50 Ci/mmol NET127005MC) were supplied by PerkinElmer Wallac (Turku, Finland). cAMP-Sp, PD98059 (1213), TBZ (2175) and okadaic acid (1136) were obtained from Tocris Bioscience (Bristol, United Kingdom). 3-hydroxybenzylhydrazine (NSD-1015, Cat. No. 54880), EDTA, HPLC standards, and other reagents were purchased from Sigma/RBI (Sigma-Aldrich Co.).

2.2. Animals

Animal experiments were conducted with 48 male Sprague-Dawley rats of 8 weeks of age, weighing 200–300 g (Animal Service, Universitat Autònoma de Barcelona, Spain or Charles River). Animals were housed two or three per cage with *ad libitum* access to food and water during a 12-h light/dark cycle. Protocols for animal handling were approved by the Ethics Committee for Human and Animal Research (Universitat Autònoma de Barcelona) in accordance with guidelines established by the Ethical Committee for the use of Laboratory Animals in Spain (53/2013) and the European Ethical Committee (2010/63/EU) and approved by the Vall d'Hebron Research Institute (VHIR) Ethical Experimentation Committee. All experiments were conducted in compliance with the ARRIVE guidelines. Surgical procedures were performed under general anesthesia using isoflurane (5% for the induction phase and 2% for the maintenance phase) (Baxter) due to its fast induction and recovery, negligible metabolism and relative sparing effect on cardiovascular function and cerebral blood flow autoregulation (Ludders, 1992). To increase DA storage, an AAV-hVMAT2 vector was injected in the morning to 8 male Charles River rats as previously stated (Carballo-Carbajal et al., 2019). No randomization was performed to allocate subjects in the study. In brief, a 10 μL Hamilton syringe with a glass capillary was used to inject 2 μL at a rate of 0.4 μL/min of the viral vector unilaterally on the right side (R) of the brain right above the substantia nigra pars compacta at the following coordinates (flat skull position), antero-posterior: −5.2 mm; medio-lateral: −2 mm, dorso-ventral: −7.6 mm, calculated relative to bregma according to the stereotaxic atlas of Paxinos and Watson (Paxinos and Watson, 1982). Then the needle was left in place for an additional 4 min period before it was slowly retracted. Rats received meloxicam 2 mg/kg after stereotaxic surgery. Continuation of analgesic treatment was decided by trained specialists who supervised animals daily to prevent and minimize any possibility of suffering, according to EU directive 2010/63/EU annex III 3.1. b. Rats were euthanized and brain tissue used 4 weeks after surgery, according to the time-line diagram shown.
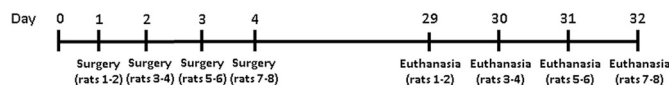
2.3. Preparation of striatal minces

Rats were euthanized by CO_2 and decapitation and brains were chilled immediately in modified Krebs-Ringer-bicarbonate medium with the following composition: 120 mM NaCl, 0.8 mM KCl, 2.6 mM $CaCl_2$, 0.67 mM $MgSO_4$, 1.2 mM KH_2PO_4, 27.5 mM $NaHCO_3$, and 10 mM glucose, pH 7.4 bubbled with 95% O_2/5% CO_2. In a 4 °C room, dorsal/medial striata from both hemispheres were dissected and sliced using a McIlwain tissue chopper obtaining tissue minces of 0.3 × 0.3 mm/side. Tissue minces were suspended in ice-cold Krebs Ringer bicarbonate medium, and washed twice by centrifugation (1000×g, 1 min, 4 °C) and resuspension in order to remove debris of damaged cells. Striatal tissue from a single rat yielded up to 28 aliquots of 25 ml each of the settled minces suspension - corresponding to 24 tissue incubations and 4 blank samples - which were randomly distributed into 2 ml polypropylene tubes containing 225 ml of ice-cold Krebs Ringer bicarbonate medium. Blank tubes were kept on ice and the rest were incubated at 37 °C and 350 rpm in an Eppendorf Thermomixer (5 Prime, Inc., Boulder, CO) under 95% O_2/5% CO_2 atmosphere. Because striatal tissue is heterogeneous, various tissue samples incubated under the same conditions

cannot be considered true "replicates", and the use of this term has been avoided. Variability between tissue incubates is due, in part, to striatal heterogeneity. Control groups comprising a minimum of 4 tissue incubations were included in every experiment. The number of tissue incubations per group is indicated in Figure legends.

2.4. Estimation of tyrosine hydroxylase activity by l-DOPA accumulation and determination of endogenous DA, DOPAC levels by HPLC-EC

The method used by Lindgren for L-DOPA accumulation in slices (Lindgren et al., 2000) was slightly modified as follows. L-DOPA was measured in two different sets of experiments depending on the presence (Fig. 1A) or absence (Fig. 1B) of a "pre-incubation" time at 37 °C before the inhibition of aromatic-L-amino-acid decarboxylase with 100 mM 3-hydroxybenzylhydrazine (NSD-1015) (properly named "incubation" where L-DOPA accumulates at a rate that is quantified in pmol mg protein^{-1} h^{-1} in Fig. 1A–B). In experiments without pre-incubation, NSD-1015 was added at the beginning of the 30-, 60- or 120-min

incubation to allow the synthesis of L-DOPA. In contrast, in experiments with pre-incubation (lasting 15, 30, 60 or 120 min) DA was synthesized before NSD-1015 addition and samples were incubated for 30 min for L-DOPA synthesis rate measurement. The accumulation of L-DOPA was quantified by HPLC with coulometric detection (HPLC-EC) (Bolea et al., 2014). A technician blinded to sample groups quantified HPLC peaks.

Tissue minces were sonicated in 0.25 M perchloric acid containing 0.25 mM EDTA and 0.1 mM sodium metabisulphite. Samples were spun in an Eppendorf microcentrifuge for 10 min, and 20 μL of supernatant were injected directly into the HPLC. The chromatography system consisted of a reversed-phase C18 column (2.5 mm particle Fortis C18, 10 × 0.46 cm, Sugelabor, Spain) and an ion-pair mobile phase, made up of 100 mM sodium phosphate buffer, 1 mM EDTA, 5 mM octanesulfonic acid (pH 2.5) plus 1% (v/v) methanol. The flow rate was 1 ml/min. This HPLC system completely separated standards of L-DOPA and DA that were detected with a Coulochem II (ESA) detector with a model 5011 dual-electrode analytical cell with porous graphite electrodes. The potential of electrodes 1 and 2 was set at −0.05 V and +0.4 V respectively.
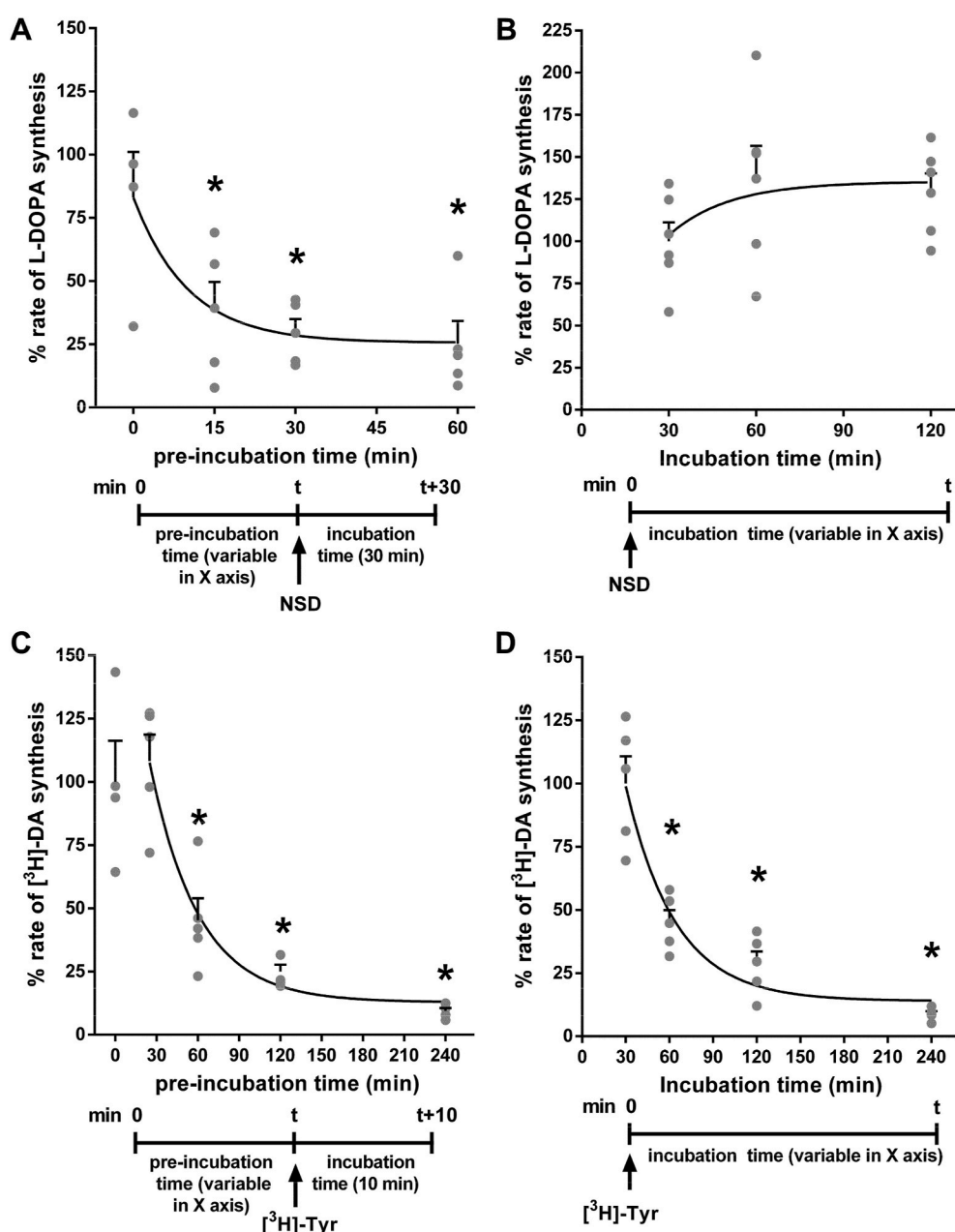
Fig. 1. Initially high L-DOPA and [³H]-DA synthesis rates decrease when DA is produced. Brain striatal minces were allowed DA synthesis (A) or not (B) by the timely addition of 100 mM NSD-1015, the decarboxylase inhibitor used to measure L-DOPA synthesis rate (A, B). The results in A were validated using a second method, where minces were incubated with [³H]-tyrosine after a pre-incubation time (C) or from the beginning of the experiment (D) to measure [³H]-DA synthesis rate. Experimental designs are shown as timelines, where "incubation" properly refers to the time period where L-DOPA synthesis from endogenous tyrosine is measured (30 min in A, x axis variable in B) or alternatively [³H]-DA synthesis from 0.12 mM [³H]-tyrosine (10 min in C, x axis variable in D). "Preincubation" refers to the previous time without NSD or [³H]-tyrosine under the same conditions. Data points and the mean ± SEM of 4–5 (A), 6 (B), 4–5 (C) or 5 (D) brain striatal tissue incubations are represented. 100% corresponds to a mean ± SEM of A) 187 ± 17; B) 10 ± 1 pmol L-DOPA/mg h; C) 257,787 ± 42,097 and D) 362,297 ± 38,857 dpm [³H]-DA/mg h. Data in (A, C and D) adjusted well to a one phase exponential decay regression curve (r² 0.91; 0.98 and 0.97 respectively). *p < 0.05, vs. respective control: A, C) 0 min; B) 30 min, ANOVA plus Dunnett's multiple comparisons test.

Detection limit was 0.2 pmol for L-DOPA. Standards of L-DOPA at different concentrations (4–400 pmol) were injected in every experiment to quantify L-DOPA by the external standard method. Sample values outside the standard range were reanalyzed or excluded. Pmols of L-DOPA were corrected by pmols present in blank samples and protein content in each sample. Results were expressed as a percentage versus control samples in each experiment. Endogenous levels of DA and DOPAC were determined in striatal mince samples with the same method. DOPAC values are shown in Fig. S1.

2.5. Purification of [3H]-tyrosine

Ring-labeled [3,5-3H]-L-tyrosine (40–60 Ci/mmol) decomposes at a rate of 1–3% per month. The main goal of this purification is to maintain a high degree of purity of commercial [3H]-tyrosine after storage. The system used for HPLC purification consisted of a reversed-phase C18 column (Tracer Extrasil ODS2, 5 mm particle size, 25 × 0.46 cm; Teknokroma, Spain) and a mobile phase with the following composition: 100 mM sodium phosphate buffer, 1 mM EDTA, 0.75 mM octanesulfonic acid (pH 3.4) and 1% (v/v) methanol. The flow rate was 1 ml/min. Under these conditions, tyrosine eluted at 9–10 min. In each purification, 0.4 mCi of [3, 5-3H]-L-tyrosine were injected into the HPLC and the whole tyrosine fraction (0.5–1 ml) was collected. The amount of [3H]-tyrosine was quantified against an external standard calibration curve of non-radiolabeled tyrosine detected by UV absorbance at 285 nm.

2.6. Purification of newly-synthesized [3H]-DA by HPLC-UV

The rate of [3H]-DA formation from 0.12 μM purified [3H]-tyrosine was measured with two experimental designs differing on the presence or absence of a pre-incubation period at 37 °C (Fig. 1C–D). In experiments without pre-incubation, purified [3H]-tyrosine was added at the beginning of the incubation for several periods of time to quantify the [3H]-DA synthesis rate. In experiments with pre-incubation, at the end of the desired pre-incubation time (usually 25, 60, 120 or 240 min at 37 °C) purified [3H]-tyrosine was added, and samples were then incubated for 10 min. "Incubation" here refers to the time when [3H]-tyrosine is transformed into [3H]-DA to quantify the synthesis rate (dpm mg prot^{-1} h^{-1}). In experiments where drugs were assayed, the timing of their addition to the incubates is indicated in the graph timelines. In all experiments, [3H]-DA synthesis was stopped by the addition of 35 ml of a deproteinizing mixture containing trichloroacetic acid (0.5% w/v), 1 mM ascorbic acid and 25 nmol non-radiolabeled DA (internal standard). Samples were homogenized in a Dynatech/Sonic Dismembrator (Dynatech Labs, Chantilly, VA). A 10 ml aliquot was taken for protein quantification by the Lowry method. Tissue homogenates were then centrifuged (12,000×g, 10 min, 4 °C), and all supernatants were processed for [3H]-DA purification by HPLC-UV. [3H]-DA formed during the incubation reaction was separated from [3H]-tyrosine by a modification of previous HPLC purification procedures used in our lab for other neurotransmitters (Ortiz et al., 2000). The chromatography system consisted of a reversed-phase C18 column (Tracer Extrasil ODS2, 5 μm particle size, 25 × 0.46 cm; Teknokroma, Spain) and an ion-pair mobile phase, made up of 100 mM sodium phosphate buffer, 1 mM EDTA, 0.75 mM octanesulfonic acid (pH 5) plus 12% (v/v) methanol. The flow rate was 1 ml/min. This HPLC system completely separates standards of tyrosine and DA detected by UV 285 nm (ring absorbance). Samples contained extremely low levels of radiolabeled tyrosine and DA that were undetectable by UV absorbance. Similarly, endogenous tyrosine and DA were negligible as compared to the amounts of internal standard DA, used to trigger [3H]-DA purification and to quantify recovery. The recovery of the internal standard in each sample (internal/external standard peak area) was quantified from internal standard DA HPLC-UV peak areas. Two ml fractions corresponding to the DA peak were recovered in scintillation vials, mixed with 6 ml Optiphase HiSafe III cocktail, and quantified in a liquid scintillation counter (PerkinElmer

Tri-Carb 2810 TR, USA) to quantify [3H]-DA. Disintegrations per minute (dpm) obtained in HPLC-purified [3H]-DA fractions were corrected by DA internal standard recovery and dpm in blank samples. Rate of [3H]-DA synthesis was estimated as the ratio of corrected dpm divided by protein content in each incubate and the incubation time in the presence of [3H]-tyrosine (dpmmg prot^{-1} h^{-1}). Results were expressed as a percentage with respect to the mean of control samples run in each experiment in order to combine data from different experiments.

2.7. Phosphorylation of tyrosine hydroxylase by Western blot

After incubation of striatal minces as described above, the Krebs-Ringer buffer was removed by centrifugation and samples were immediately frozen (−80 °C). After thawing samples were homogenized in 100 μl of ice-cold lysis buffer (1 mM orthovanadate, 50 mM Tris-HCl pH 7.5, 25 mM sodium pyrophosphate, 50 mM NaCl, 1% Triton X100, 50 mM sodium fluoride, 5 μM zinc chloride, 2 mM DTT, phosphatase inhibitor cocktail 1 (Sigma) and protease inhibitor cocktail 1 (Sigma). Equal amounts of protein were separated by SDS-PAGE electrophoresis followed by transference in polyvinylidene fluoride membrane at 100 V for 1 h. The blotting buffer used contained 25 mM Tris, 200 mM glycine and 10% methanol (v/v). Membranes were blocked for 1 h with Tris-buffered saline, supplemented with 0.1% Tween 20 and 5% (w/v) defatted milk powder. Then, the membranes were incubated overnight with the indicated antibody diluted in blocking buffer. The primary antibodies against tyrosine hydroxylase (1:2500, AB5280), phosphoSer31-TH (1:1000, AB5423) and phosphoSer40-TH (1:1000, AB5935) were obtained from Millipore. Monoclonal antibody against β-actin was from Sigma-Aldrich (1:4000, clone AC-74). Cell Signaling Technology antibodies against ERK-1/2 (1:1000, 9102) and against dually phosphorylated (Thr202/Tyr204) ERK-1/2 (1:1000, 9101) were used. The secondary horseradish peroxidase-conjugated antibodies used were goat anti-mouse (1:1000, 172–1011) from Bio-Rad and goat anti-rabbit (1:1000, 31460) from Pierce. Signals were obtained using a ChemiDoc device (Bio-Rad) and quantitative analysis was performed using the ImageLab software (Bio-Rad). Results were expressed as pTH/TH ratio of standardized optical density determined within each blot.

## 2.8. Tyrosine hydroxylase immunoprecipitation, in-gel peptide digestion and LC-MS/MS analysis

TH was immunoprecipitated using 10 μg anti TH antibody (Millipore AB5280) and Pierce Crosslink Magnetic IP/Co-IP Kit (Thermo Fischer 8885) from 4 h-incubated striatal minces and non-incubated ice controls from two animal brains. SDS-PAGE bands revealed with Coomasie blue were manually excised and digested with trypsin using a DigestPro MS digestor (Intavis). The process involved reduction with DTT, derivatization with iodoacetamide, and enzymatic digestion with trypsin at 37 °C for 8 h (Casanovas et al., 2009). The resulting peptide mixtures were evaporated to dryness and redissolved in 20 μL 5% MeOH, 0.5% TFA. Peptides were analyzed by LC-MS/MS using a 1200 HPLC system (Agilent Technologies, Santa Clara, CA, USA) coupled to an LTQ Orbitrap XL mass spectrometer (Thermo Scientific) equipped with a nano-electrospray source (Proxeon, Odense, Denmark). Samples were separated with a C18 pre-concentration cartridge (Agilent Technologies) connected to a C18 100 μm × 150 mm column (Nikkyo Technos Co, Tokyo, Japan) at 400 nL/min using a 30-min linear gradient from 0 to 35% solvent B (Solvent A: water, 0.1% (v/v) formic acid; solvent B: acetonitrile, 0.1% (v/v) formic acid). The LTQ XL Orbitrap was operated in the positive ion mode with a spray voltage of 1.8 kV. The spectrometric analysis was performed in a data-dependent mode, acquiring a full scan followed by 8 MS/MS scans of the 8 most intense signals from the inclusion list (see Supplementary Table S1). If an ion resulting from a neutral loss of phosphate from the precursor ion (loss of 49, 32.6, 24.5 uma) was detected among the 3 most abundant fragments in the MS/MS spectrum, a MS3 scan was performed on this ion. The full scan spectra

(scan range m/z 400–1650) were acquired in the Orbitrap with a resolution of 60.000 (at m/z 400). The MS/MS spectra were acquired in the linear ion-trap. For relative quantification, the area of each monitored peptide was calculated using the Xcalibur software (Thermo Scientific).

2.9. Experimental Design and Statistical Analysis

The study was not pre-registered. No sample calculation or blinding was performed. No animals were excluded, but undetectable protein levels in samples was considered an exclusion criterion. Control groups with a balanced number of brain striatal tissue incubations (at least 4) were included in every experiment. In [^{3}H]-DA and L-DOPA synthesis rate experiments, raw data of control incubations are given in each figure legend. Once normalized to 100% of basal synthesis in each experiment, data were pooled to increase the total number of incubations represented in graphs and used for statistics. Thus graphs represent incubation samples that may be obtained from different animals, which is important due to the limited amount of brain striatal tissue per animal and its inherent heterogeneity. As stated before, the use of the term "replicates" has been avoided to stress the heterogeneity of tissue minces randomly assigned to each treatment group. Statistical analysis was carried out with GraphPad Prism software (v6, GraphPad Software Inc, USA). Normality was assessed with the Shapiro-Wilk normality test. The ROUT test (Q = 1%) was used to detect those data points that can be considered statistical outliers and that should be excluded from analysis. Two-way ANOVA was used to analyze the interaction between different factors on synthesis rate (e.g., time, treatment or concentration of DA as factors). Statistical significance of differences vs. control group was assessed by Dunnett's multiple comparisons test while Sidak's was used to evaluate differences between treatments. Differences were considered statistically significant if the probability of error was less than 5%.
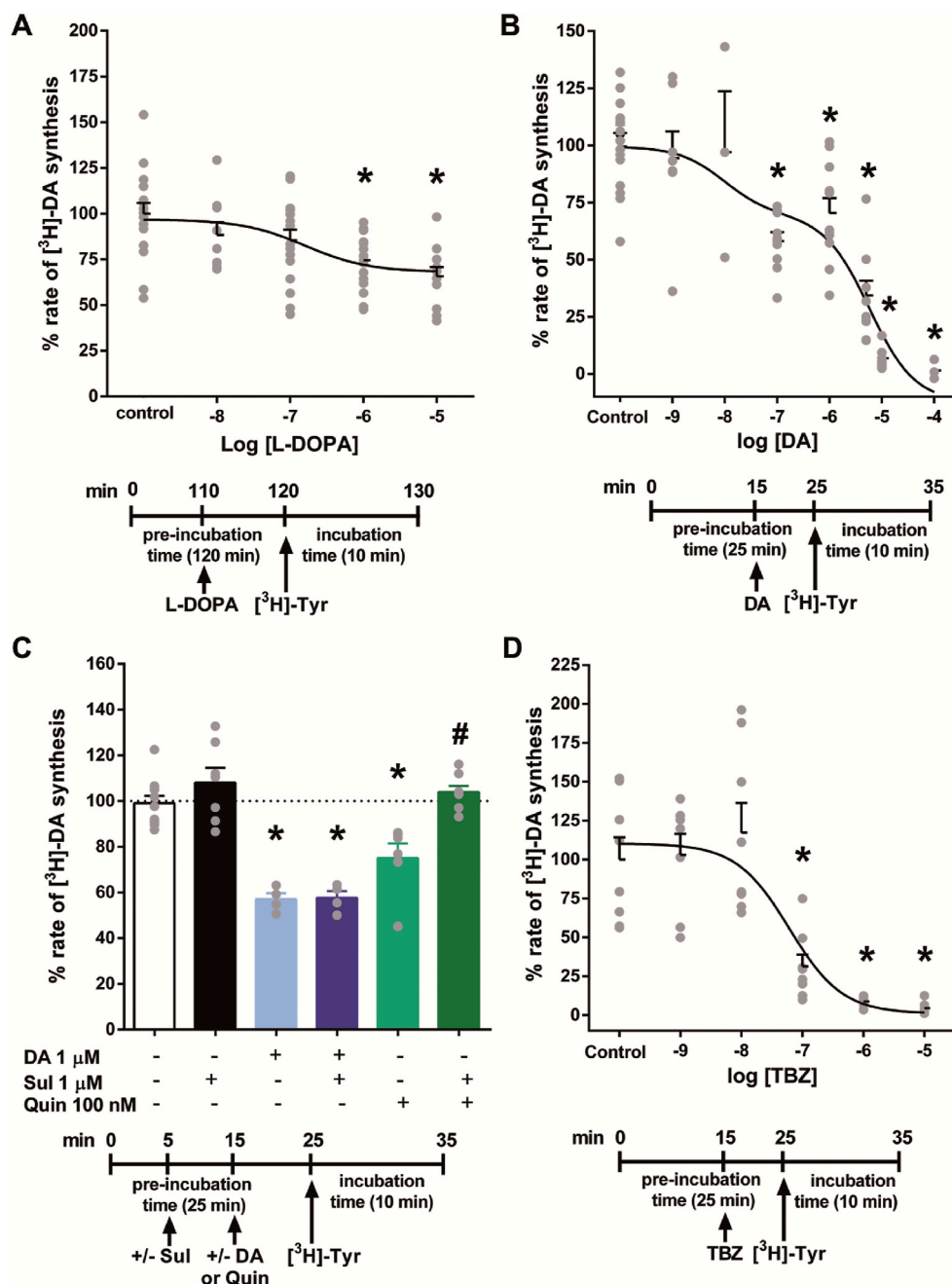

Fig. 2. [^{3}H]-DA synthesis rate is controlled by non-stored DA as well as by D$_2$-like receptor dependent mechanisms. Increases in intracellular DA were sought by adding increasing concentrations of L-DOPA (A), DA (B) or the VMAT2 inhibitor TBZ (D) to brain striatal minces. In C, either 1 μM DA or the D$_2$-like receptor agonist quinpirole were applied, but only quinpirole effects were blocked by the D$_2$-like receptor antagonist sulpiride. Experimental designs until measurement are shown as timelines below each graph. Data points and the mean ± SEM of 9–17 (A), 3–18 (B), 4–11(C) and 6–8 (D) brain striatal tissue incubations are represented. In B) 4 incubations were excluded from the analysis after values were considered outliers by the ROUT test. Dose-response curves adjusted to one site competition (A, IC$_{50}$ 1.6x10^{-7} M; r^2 0.95), two-site competition (B, IC$_{50}$ 9.3x10^{-9} M and 5.8x10^{-6} M; r^2 0.97; p < 0.005 vs. one-site competition) and one-site competition (D, IC$_{50}$ 6.1x10^{-8} M; r^2 0.96) respectively. 100% corresponds to a mean ± SEM of A) 60,151 ± 4784; B) 295,539 ± 17,413; C) 62,946 ± 2684 and D) 617,245 ± 99,937 dpm [^{3}H]-DA/mg.h. A, B, D). *, p < 0.05, vs. respective control; ANOVA plus Dunnett's multiple comparisons test. C) Two-way ANOVA showed a significant effect of treatment (F (2,34) = 42.2; p < 0.0001) and Sulpiride presence (F(1,34) = 10.4; p < 0.005), and a significant interaction between these two factors (F(2,34) = 4.4 p < 0.05); *, p < 0.05, vs. group without treatment; #, p < 0.05 vs. Quin 100 nM, Two way ANOVA plus Sidak's multiple comparisons test.

3. Results

3.1. De novo DA synthesis is necessary and sufficient to trigger spontaneous end-product inhibition of TH

With the aim of analyzing DA feedback-inhibition of TH activity, we modified the method of L-DOPA accumulation after decarboxylase inhibition with 100 mM NSD-1015 applied to slices (Lindgren et al., 2000) (Fig. 1A–B). To allow *de novo* DA synthesis we pre-incubated tissue for up to 60 min at 37 °C before NSD-1015 addition. We observed a decrease of L-DOPA synthesis rate with pre-incubation time (Fig. 1A) fitting to a one-phase exponential decay regression curve (maximal decrease 80%). The presence of NSD-1015 from the beginning of the incubation prevented decreases in the rate of L-DOPA
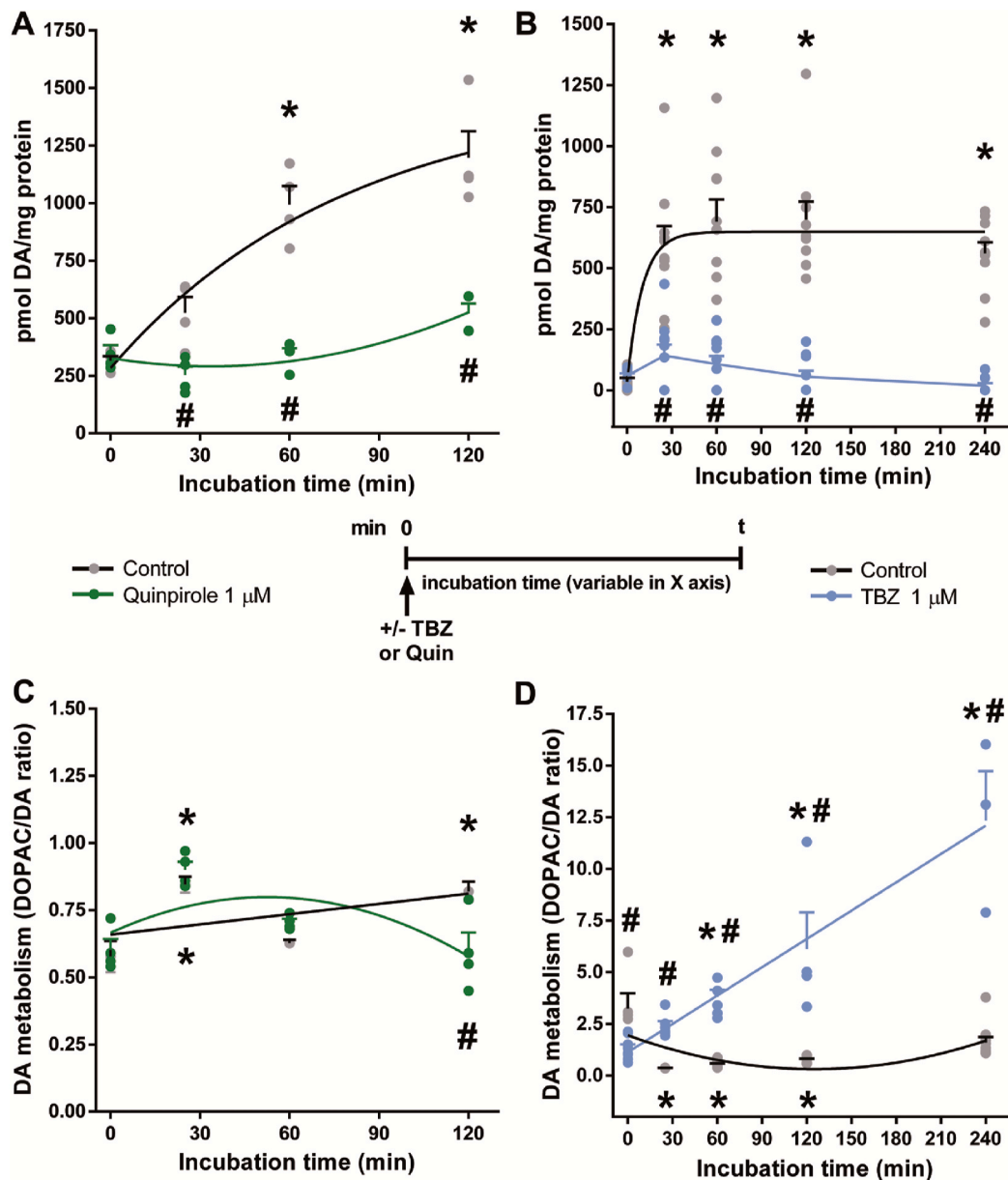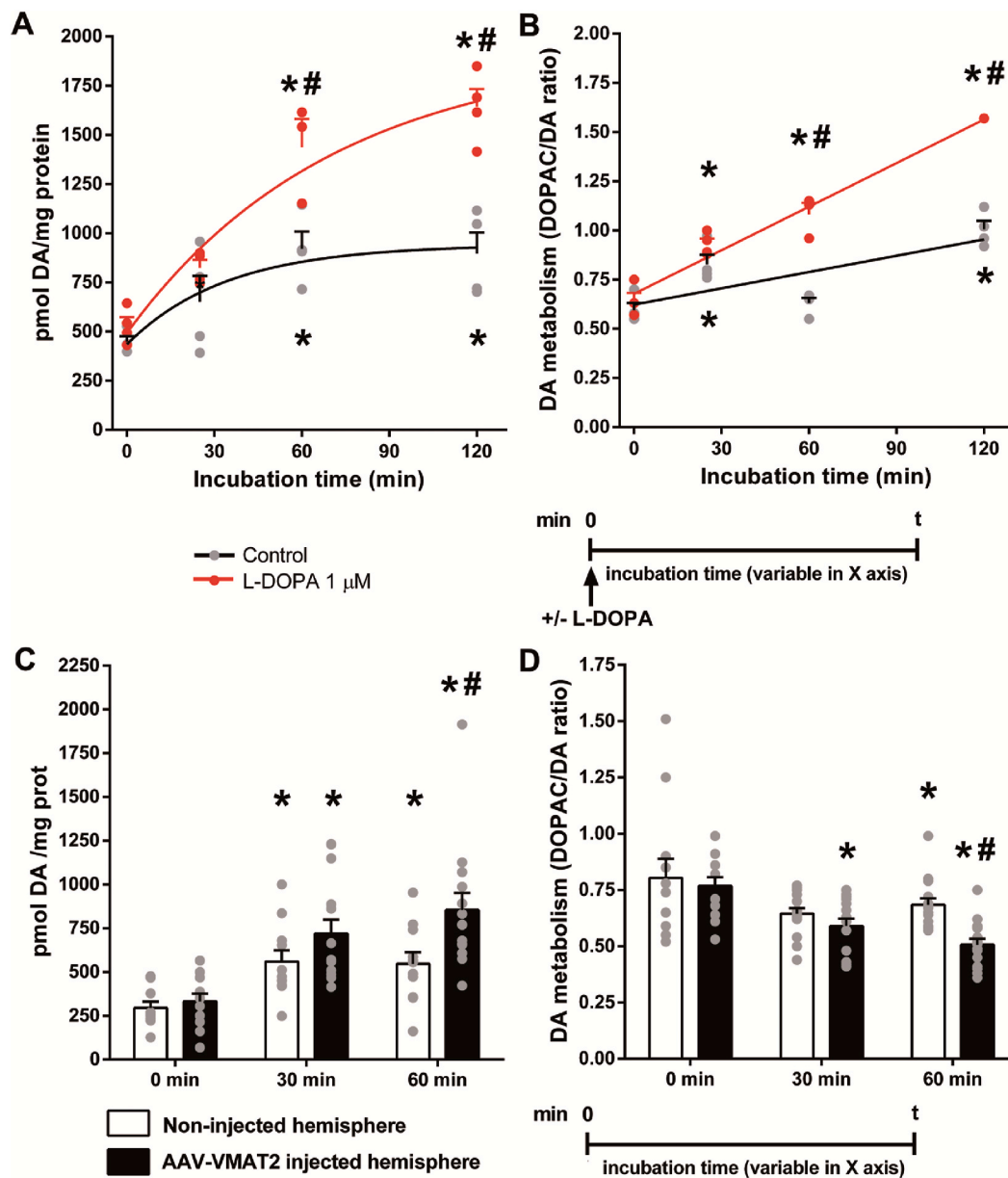

Fig. 3. Endogenous DA concentrations increase spontaneously with incubation time if DA synthesis and storage are not impaired. DA accumulated during the incubation of brain striatal minces (A, B, black lines) unless D$_2$-like autoreceptors were stimulated with 1 μM quinpirole (A, green line) or the VMAT2 inhibitor TBZ 1 μM (B, blue line) was present. The DOPAC/DA ratio index of DA metabolism increased with TBZ (D), but not with quinpirole (C) treatments or in control conditions (C, D, black lines). The experimental design is shown in the timeline. Data and the means ± SEM of N equal to A) 4 (control), 4 (Quin); B) 6–10 (control), 9–10 (TBZ); C) 3–4 (control), 4 (Quin); D) 5–10 (control), 3–8 (TBZ) brain striatal tissue incubations are represented. In B) 1 and D) 4 incubations were excluded from the analysis after values were considered outliers by the ROUT test. Control curves of DA accumulation (A, B) adjusted to a one-phase association curve (r^2 0.96 and 0.95, respectively) while those of DOPAC/DA ratio (C, D) fit to a linear (r^2 0.81) and a second order polynomial (r^2 0.97) equations, respectively. This latter regression was also followed by Quin in both A) and C) (r^2 0.92 and 0.85, respectively). TBZ effects on D) followed a linear regression (r^2 0.97). Two-way ANOVA showed in A) a significant effect of Treatment (F$_{(1,24)}$ = 81.6; $p < 0.0001$) and Time (F$_{(3,24)}$ = 32.3; $p < 0.0001$), and a significant interaction between these two factors (F$_{(3,24)}$ = 15.3 $p < 0.0001$); in B) a significant effect of Treatment (F$_{(1,85)}$ = 161.3; $p < 0.0001$) and Time (F$_{(4,85)}$ = 11.8; $p < 0.0001$), and a significant interaction between these two factors (F$_{(4,85)}$ = 10.1 $p < 0.0001$); in C) a significant effect of Time (F$_{(3,23)}$ = 16.1; $p < 0.0001$), and a significant interaction between time and treatment (F$_{(3,23)}$ = 5.5 $p < 0.005$) and in D) a significant effect of Treatment (F$_{(1,60)}$ = 141.5; $p < 0.0001$) and Time (F$_{(4,60)}$ = 36.3; $p < 0.0001$), and a significant interaction between these two factors (F$_{(4,60)}$ = 40.4 $p < 0.0001$); *$p < 0.05$, vs. 0 min, ANOVA plus Dunnett's multiple comparisons test; #$p < 0.05$, vs. data in control curve, ANOVA plus Sidak's multiple comparisons test.

accumulation with incubation time (Fig. 1B). As NSD-1015 blocks the aromatic-L-amino-acid decarboxylase, preventing new DA production, this result likely indicated that DA feedback-inhibition was responsible for the decay of TH activity. To confirm this result, we used a second method to determine DA synthesis without NSD-1015, based on the HPLC purification of $[^3H]$-DA after incubation of tissue minces with $[^3H]$-tyrosine. Again, a time-dependent decay in $[^3H]$-DA synthesis rate was observed consistent with new DA formation. The decrease adjusted

to a one phase exponential decay regression curve either with or without pre-incubation before $[^3H]$-Tyr was added with similar results (Fig. 1C and D). $[^3H]$-DA synthesis rate appeared maximal between the initial 0 and 25 min of pre-incubation time.

Next, we studied the effects of exogenous L-DOPA or DA. The addition of L-DOPA further reduced the rate of $[^3H]$-DA synthesis in a concentration-dependent manner (Fig. 2A). The addition of DA also decreased $[^3H]$-DA synthesis rate in a concentration-dependent manner

Fig. 4. Endogenous DA vesicular storage and metabolism is altered by exogenous L-DOPA and VMAT2 overexpression. L-DOPA addition to brain striatal minces increased DA concentrations (A) and metabolism (B) while VMAT2 overexpression increased DA storage (C) but decreased DA metabolism (D). Incubation designs are shown as timelines: In A, B) variable incubation times with addition of 1 μM L-DOPA at the beginning of incubation; C-D) no incubation, 30- or 60-min incubation of left or right striatum one month after the injection of AAV-hVMAT2 viral vector unilaterally in the right substantia nigra. Data represent the endogenous DA values and DOPAC/DA ratio and the means ± SEM of N equal to A, B) 4 (control), 3–4 (L-DOPA); C) 13–14 (non-injected), 13–16 (injected); D) 12–15 (non-injected), 12–15 (injected) brain striatal tissue incubations. In B) 1 and C) 5 incubations were excluded from the analysis after values were considered outliers by the ROUT test. Control and L-DOPA curves adjusted to A) a one-phase association curve (r^2 0.89 and 0.97, respectively) and B) linear regression (r^2 0.89 and 0.98, respectively). Two-way ANOVA showed in A) a significant effect of Treatment ($F(1,23) = 35.5$; $p < 0.0001$) and Time ($F(3,23) = 34.2$; $p < 0.0001$), and a significant interaction between these two factors ($F(3,23) = 6.1$ $p < 0.0001$); in B) a significant effect of Treatment ($F(1,22) = 112.5$; $p < 0.0001$) and Time ($F(3,22) = 99.8$; $p < 0.0001$), and a significant interaction between these two factors ($F(3,22) = 21.3$ $p < 0.0001$); in C) a significant effect of Treatment ($F(1,65) = 7.8$; $p < 0.01$) and Time ($F(2,65) = 15.1$; $p < 0.0001$) without a significant interaction between these factors and in D) a significant effect of Treatment ($F(1,78) = 7.1$; $p < 0.01$) and Time ($F(2,78) = 11.8$; $p < 0.0001$), without a significant interaction between these factors; *$p < 0.05$, vs. 0 min, ANOVA plus Dunnett's multiple comparisons test. #$p < 0.05$, vs. respective control: A, B) data in control curve; C-D) non-injected hemisphere, ANOVA plus Sidak's multiple comparisons test.

(Fig. 2B). DA effect adjusted well to a two-site competition curve (IC_{50} $9.3x10^{-9}$ M and $5.8x10^{-6}$ M; r^2 0.97; $p < 0.005$ vs. one-site competition). 100 μM DA completely abolished [^{3}H]-DA synthesis rate. D_2 receptor stimulation did not explain the effects of 1 μM DA, as DA effects were not blocked by the D_2-like receptor antagonist sulpiride (Fig. 2C). Nevertheless, as a positive control we checked whether D_2-like receptors were functional in our brain minces. Indeed, the agonist quinpirole (100 nM) did produce a significant reduction in [^{3}H]-DA synthesis rate (Fig. 2C) that was completely antagonized by pre-incubation with 1 μM sulpiride (Fig. 2C). Next, we tested whether intracellular DA was involved in the [^{3}H]-DA synthesis decrease through manipulating DA storage with the VMAT2 inhibitor tetrabenazine (TBZ). As expected, TBZ produced a concentration-dependent decrease of [^{3}H]-DA synthesis rate (IC_{50} $6.1x10^{-8}$ M; one-site competition, r^2 0.96) (Fig. 2D). 1 μM TBZ completely impaired DA synthesis. These findings indicate that non-stored DA negatively feeds-back on the TH enzyme, and DA storage dynamics strongly influence DA biosynthesis.

3.2. DA storage dynamics

The striking dependence of DA synthesis rate on incubation time *ex vivo* led us to evaluate endogenous DA levels on the same time frame. Unexpectedly, we found that endogenous DA levels in brain striatum markedly and spontaneously increased during incubation, approaching a plateau after 60 min (Fig. 3A and B). The kinetics of this spontaneous DA accumulation in tissue *ex vivo* led us to hypothesize that the initially high rate of DA synthesis becomes more moderate as DA storage in vesicles approached saturation. To test this hypothesis, we conducted several experiments interfering with DA synthesis or storage and determining endogenous DA levels. First, as expected, addition of the aromatic-L-amino-acid decarboxylase inhibitor NSD-1015 (100 mM) completely prevented the time-dependent increase in DA levels, or even decreased them (ice control: 244 ± 69 pmol DA/mg protein; 2 h incubated in the presence of NSD-1015: 144 ± 32 pmol DA/mg protein, mean ± S.D., N = 6/group). Second, incubation time-dependent dopamine accumulation *ex vivo* was greatly reduced by the presence of the D_2 receptor agonist quinpirole (1 μM) during the 2 h incubation (Fig. 3A, green line). Third, the VMAT2 inhibitor tetrabenazine (1 μM) completely impaired DA accumulation (Fig. 3B, blue line) as expected by blockade of DA storage. However, differences in the mechanisms of action of quinpirole and TBZ were evident by their differential modulation of the DOPAC/DA ratio. Quinpirole did not increase the DOPAC/DA ratio (Fig. 3C, green line) suggesting the drug slowed down new DA biosynthesis, while TBZ resulted in a clear time-dependent increase DOPAC/DA ratio (Fig. 3D, blue line) revealing increased metabolism of non-stored DA.

Treatments increasing DA storage were also used. The presence of 1 μM L-DOPA during incubation increased both DA accumulation (Fig. 4A) and the DOPAC/DA ratio (Fig. 4B) time-dependently. On the other hand, enhancement of VMAT2 expression by the previous unilateral injection of the hVMAT2 viral vector in the right substantia nigra increased ipsilateral striatal DA concentration (Fig. 4C) and decreased DOPAC/DA ratio (Fig. 4D) when compared with the contralateral side. These effects were only evident after a 60 min incubation, as both hemispheres showed incubation time-dependent effects. Thus, VMAT2 over-expression also increased DA storage but, differently to L-DOPA addition, it decreased DA metabolism. All these results support the hypothesis that the accumulation of newly formed DA in the cytosol is responsible of the observed decay of [^{3}H]-DA biosynthesis with time. Moreover, the spontaneous increase in endogenous DA levels (Fig. 3A–B, black line) without a concomitant alteration of the DOPAC/DA ratio (Fig. 3C–D, black line) indicated us that this tissue preparation was actively synthesizing and storing DA, likely until maximal storage was reached. Thus, we asked if this phenomenon could be generalized to another neurotransmitter. Serotonin (5-HT) levels showed also a clear pattern of incubation time-dependent accumulation *ex vivo*, both in the

striatum and hippocampus (Fig. 5). New biosynthesis of DA and 5-HT seems then to nearly fill vesicular stores during the first 2 h of tissue slice incubation *ex vivo*.

3.3. TH phosphorylation status

TH activity is known to be regulated in the short-term by changes in its phosphorylation state (Haycock and Haycock, 1991). TH can be phosphorylated at several serine residues by protein kinases such as PKA, ERK or CaMKII, and it can be dephosphorylated by PP2A and PP2C protein phosphatases (for review see (Dunkley et al., 2004)). A 25 min incubation with the MEK inhibitor PD98059 50 μM decreased [^{3}H]-DA synthesis, while increased [^{3}H]-DA synthesis resulted from PKA activation with 1 mM cAMP-Sp or Ser/Thr protein phosphatases inhibition with Ok 1 μM (Fig. 6A). Interestingly, a time-dependent decay of [^{3}H]-DA synthesis rate was still observed during all these treatments. Either endogenous (Fig. 6A, time effect) or exogenous DA (Fig. 6B) were able to decrease [^{3}H]-DA synthesis under the influence of agents able to alter TH phosphorylation.

TH phosphorylation and TH protein amounts were also monitored. In separate experiments, TH phosphorylation in Ser31 and in Ser40 vs. total TH was determined by Western blot at different incubation time points up to 240 min. β-actin was used as an additional loading control of total TH levels. No clear effects of incubation time on TH phosphorylation were apparent (Fig. 7A, B and C). In contrast, treatment with 1 μM Ok induced a transient two-fold increase in phosphoSer31-TH, reaching the highest point at 120 min (Fig. 7B), and a delayed effect in phosphoSer40-TH, reaching the highest point at the longest time analyzed (240 min, Fig. 7C). Importantly, total TH protein was not decreased during the overall incubation time (Fig. 7A and D and S3). Thus, although Ok increased both [^{3}H]-DA synthesis rate and TH phosphorylation as expected, TH levels or phosphorylation status did not decay time-dependently either in the absence or presence of Ok. In addition, the ratio between TH and actin was also measured, showing no changes at any time of incubation with or without Ok (Supplementary Fig. S3).

25 μM PD98059 did not change phosphoSer31 in TH at the shortest incubation times (Fig. 7E) despite 50 μM decreased [^{3}H]-DA synthesis as soon as 25 min of incubation (Fig. 6A). A positive control of the effectiveness of 25 μM PD98059 was performed by detection of phosphoERK-1/2 in Thr202 and in Tyr204 by Western blot. 25 μM PD98059 decreased ERK-1/2 phosphorylation ratio vs. total ERK-1/2, as expected for a MEK inhibitor, but only after 60 min of incubation (Fig. 7D). Since Ser31-TH phosphorylation in brain does not seem to undergo major changes during incubation (Fig. 7E), the DA feedback on TH we observe also seems unrelated to Ser31- TH phosphorylation.

In order to further search possible changes of the TH phosphorylation status on Ser31 and Ser40 due to brain tissue incubation *ex vivo*, we used mass spectrometry (Fig. 8). Total TH was immunoprecipitated in parallel from 4 h-incubated striatal minces (Fig. 8B) and ice controls (Fig. 8A, not incubated) obtained from the same animal brain. Trypsin digestion of TH immunoprecipitated samples yielded peptides unequivocally recognized as TH fragments. The ratio of Ser31 phosphorylated vs. non-phosphorylated peptides was almost unchanged (28% in ice control and 25% in 4 h incubation). Ser40 phosphorylation was much lower than Ser31, and not decreased by time (1.1% in ice control, 2% after 4 h incubation). Thus, mass spectrometry confirmed the main Western blot results: incubation time did not alter TH phosphorylation in Ser31 and Ser40, and Ser31 was significantly phosphorylated during the whole incubation. In addition, Ser19 phosphorylation could be detected (25% in ice control vs. 18% in the 4 h-incubated sample, % relative to the unphosphorylated peptide). Furthermore, Thr30 phosphorylation was also detected (12% in ice control vs. 14% in 4 h-incubated sample). To our knowledge, this is the first report of TH phosphorylation in Thr30.

In conclusion, the time-dependent decay of [^{3}H]-DA synthesis rate
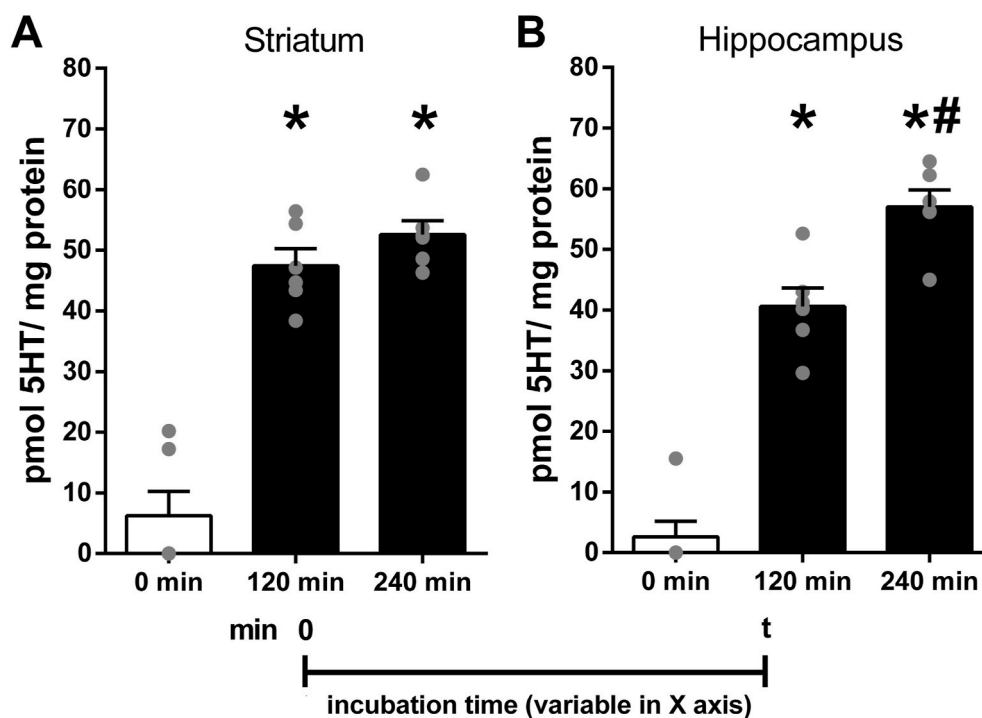
Fig. 5. Like DA, endogenous serotonin (5-HT) concentrations also increase spontaneously with incubation time. 5-HT levels in the striatum (A) and hippocampus (B) showed a clear pattern of incubation time-dependent accumulation *ex vivo*. 0 min bars show non-incubated ice controls. Data represent the endogenous 5-HT values and the means $\pm$ SEM of N = 6 brain tissue incubations/group. *$p < 0.05$, vs. 0 min, #$p < 0.05$, vs. 120 min; one-way ANOVA plus Tukey's multiple comparisons test.

was not due to TH degradation or to a loss of Ser31-or Ser40-TH phosphorylation over time. Agents altering Ser31-or Ser40-TH phosphorylation modified the pattern - but did not prevent - of the time-dependent decay of TH activity. Inability to further store DA is the main factor involved in the decrease of TH activity with incubation time.

4. Discussion

We report that DA inhibition of brain TH activity is strongly dependent on DA storage, and it is measurable in fresh brain *ex vivo*, by using a simple approach to assess dopamine synthesis and storage dynamics.

TH inhibition by DA feedback has long been known, but often overlooked. The popularity of methods to determine brain TH activity based in L-DOPA accumulation should have contributed to its neglection, as pharmacological blockade of aromatic-L-amino-acid decarboxylase prevents DA formation and thus feedback. During the set-up of this technique, we found a time-dependent decrease of brain TH activity (Figs. 1–2) associated to a pattern of spontaneous DA accumulation (Figs. 3 and 4) clearly indicating new DA formation and storage. When DA storage eventually approached saturation of vesicles, non-stored DA was likely free to inhibit TH in the cytosol, decreasing TH activity. Although these findings could be rationally expected, we did not anticipate observing them so clearly by using our simple methodology. Tissue manipulation was limited to chop a fresh brain striatum, wash and incubate it in non-depolarizing Krebs buffer. Hence striatal minces maintained most structure and functionality after probably losing part of its dopamine content during CO_2 euthanasia and tissue chopping. Brain incubation at 37 °C restored a -transiently- hyperactive DA synthesis in catecholaminergic pre-synaptic varicosities or terminals until storage in vesicles reached its maximal capacity. A straightforward HPLC purification of [³H]-DA, or the quantification of endogenous DA, L-DOPA and DOPAC, completed the procedures. In our non-depolarizing conditions (2 mM K⁺) the release of newly formed [³H]-DA to the extracellular medium is very low (approximately 1% of total [³H]-DA synthesis (Ma

et al., 2014)) and at least 90% of newly formed DA may be stored in vesicles (Eisenhofer et al., 2004). The DA increase with time under non-depolarizing conditions agrees with previous reports of increased TH activity after cessation of neuronal firing (Aghajanian and Roth, 1970; Andén et al., 1973; Walters et al., 1973). Using computer simulations, Wallace (2007) predicted that DA negative feedback on TH would not occur in the presence of efficient DA storage and the absence of release and reuptake, explaining transiently hyperactive dopamine biosynthesis at the beginning of the incubation. When vesicles approach saturation, storage becomes less efficient and DA spillover may happen, leading to the decay in TH activity. Accordingly, the decrease of TH activity was dependent on new DA synthesis (Fig. 1) and storage (Figs. 2–4), and we ruled out other alternatives. Firstly, we discarded the possibility of a depletion of endogenous tyrosine levels, as [³H]-tyrosine was provided for [³H]-DA synthesis at different times (Fig. 1C–D and 2). In addition, a depletion of endogenous tyrosine cannot explain the time-dependent DA accumulation (Figs. 3 and 4). Secondly, we rejected the possible activation of DA degradation pathways because the DOPAC/DA ratio remained stable (Fig. 3C–D, black line). Finally, we also rejected the hypothesis that time dependent changes obeyed to a loss of TH phosphorylation (Figs. 7 and 8) or D_2 autoreceptor activation (Fig. 2C).

Impairment of vesicular uptake with TBZ prevented TH activity presumably by enhancing cytosolic DA. Dopamine D_2 activation by quinpirole prevented TH activity through signal transduction mechanisms. Although in both cases DA accumulation was impaired (Fig. 3), only TBZ increased DOPAC levels showing increased DA metabolism. These results support the involvement of new DA synthesis and storage on DA accumulation. Traditionally, the DOPAC/DA ratio has been considered to reflect metabolism by monoamine oxidase (MAO). We found clear increases of DOPAC/DA ratio with TBZ and L-DOPA (Figs. 3–4), which shows that insufficient DA storage leads to metabolism. In the presence of L-DOPA, DA storage could reach a higher maximum as it can also involve non-dopaminergic cells in brain striatum able to decarboxylate L-DOPA and store DA. Accordingly, VMAT2
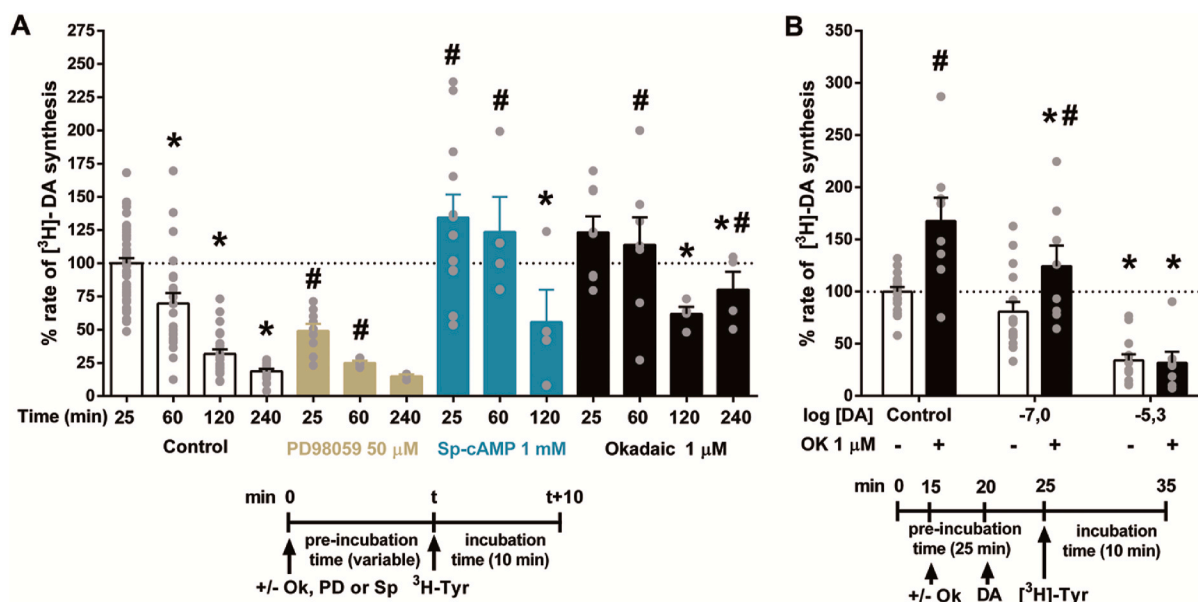
Fig. 6. DA and phosphorylation agents modulate TH activity. The decay of [³H]-DA synthesis rate with time (A) was evaluated in brain striatal minces under the effects of agents that modify TH phosphorylation state such as PD98059, a MEK/ERK pathway inhibitor; Sp-cAMP, a PKA activator; and okadaic acid (Ok), a phosphatase inhibitor. Drugs were added at the beginning of the pre-incubation time indicated in the x-axis and timeline, plus 10 min incubation with [³H]-Tyr properly used to measure [³H]-DA synthesis rate. The effects of 1 μM Ok (B) were further evaluated in combination with 0.1 and 5 μM DA. Addition of the compounds to brain striatal tissue is indicated in timelines. Data represent individual incubation values and mean ± SEM % of control [³H]-DA synthesis at 25 min (A) of N equal to 14–50 (control), 3–9 (PD98059), 4–12 (Sp-AMPc) and 4–8 (Ok) tissue incubations or (B) mean ± SEM of N equal to 16–18 (control) and 7–8 (OK) tissue incubations. 1 incubation in (A) was excluded from the analysis after the value was considered outlier by the ROUT test. In control groups 100% corresponds to a mean ± SEM of 632,898 ± 87,744 (A) and 295,539 ± 17,413 (B) dpm [³H]-DA/mg.h. Two-way ANOVA showed in A) a significant effect of Treatment ($F(1,96) = 16.4$; $p < 0.0001$) and Time ($F(2,96) = 18.4$; $p < 0.0001$), without a significant interaction between these factors for PD98059; a significant effect of Treatment ($F(1,111) = 15.9$; $p < 0.0001$) and Time ($F(2,111) = 23.7$; $p < 0.0001$ without a significant interaction between these factors for Sp-cAMP; and a significant effect of Treatment ($F(1,126) = 32.6$; $p < 0.0001$) and Time ($F(3,126) = 22.8$; $p < 0.0001$) without a significant interaction between these factors for Ok. In B) two-way ANOVA showed a significant effect of Treatment ($F(1,67) = 15.5$; $p < 0.0005$) and DA concentration ($F(2,67) = 40.8$; $p < 0.0001$), and a significant interaction between these two factors ($F(2,67) = 4.9$ $p < 0.05$). A) *$p < 0.05$ vs. respective 25 min pre-incubation, ANOVA plus Dunnett's multiple comparisons test. #$p < 0.05$ vs. control group, ANOVA plus Sidak's multiple comparisons test. B) *$p < 0.05$vs. respective control, ANOVA plus Dunnett's multiple comparisons test. #$p < 0.05$ vs. non-treated groups, ANOVA plus Sidak's multiple comparisons test.

overexpression raised DA storage and decreased the DOPAC/DA ratio (Fig. 4C–D). DA metabolism to DOPAC increased modestly with time when maximal storage was reached, as DA levels in the cytoplasm likely approached the high μM MAO Km (Best et al., 2009). However, the increase of DA metabolism must have been limited by DA feedback on TH. It is of note that 5-HT also accumulated time-dependently even more clearly than DA (Fig. 5), which may be due to the lack of a negative feedback of 5-HT on tryptophan hydroxylase.

Inhibition of [³H]-DA synthesis by exogenous DA fits with a two-site competition regression, with approximate IC₅₀ of 20 nM and 4 μM for high- and low-affinities respectively (Fig. 2B). These results support previous *in vitro* studies (Dickson and Briggs, 2013; Gordon et al., 2008) suggesting the existence of two DA binding sites or TH conformations with high and low affinities (K_D 4 nM and 90 nM respectively) (Gordon et al., 2009; Nakashima et al., 2009; Tekin et al., 2014) although we cannot discard additional explanations, especially for the low DA affinity. Quantitative differences between our results and previous publications could be due to the need for exogenous DA to enter the tissue (i. e., through the DA or other transporters) and to the inherent complexity and heterogeneity of brain slices. Without an actual measure of cytosolic DA -difficult to obtain experimentally-it would be speculative to suggest which of the DA binding sites/conformations were occupied by DA in each condition assayed. Nevertheless, if we consider that cytosolic DA concentration may be lower than 100 nM (Mosharov et al., 2006), the high-affinity binding site/conformation might be almost completely occupied by DA. In contrast, the low-affinity binding site/conformation would putatively be the one able to respond to a further increase in cytosolic DA concentrations due to inefficient vesicle storage. Further

work could better address this issue, e.g. by using mutant TH insensitive to feedback inhibition by dopamine (Mor et al., 2017). Cell cultures where intracellular amperometric recordings measure dopamine vesicular content would also be helpful to better understand dopamine dynamics (Gu and Ewing, 2021) under non-depolarizing (this work) or depolarizing conditions.

In basal physiological conditions less than 5% of TH is phosphorylated in Ser40 (Dunkley et al., 2004; Dunkley and Dickson, 2019). This low value agrees with the 1–2% signal ratio of phosphorylated/unphosphorylated Ser40-TH peptides we find by mass spectrometry (Fig. 8), as mass spectrometry signals depend both on peptide abundance and ionization efficiency, the latter being lower when peptides are phosphorylated. Ser40-TH phosphorylation has been reported to increase affinity for tetrahydrobiopterin (BH₄) cofactor and to decrease high-affinity DA binding (Daubner et al., 2011; Ramsey and Fitzpatrick, 1998). The low percentage of Ser40-TH phosphorylation suggests DA normally occupies the high-affinity site/conformation, and basal TH activity is supposed to be low. Nevertheless, TH was very active when newly synthesized DA was being stored in vesicles at the beginning of the incubation. Again, the low percentage of Ser40-TH phosphorylation suggests that cytosolic DA (newly synthesized, leaking from vesicles, or exogenously added and re-uptaken) may exert its inhibitory effect through the low-affinity binding site/conformation of TH. In accordance with previous reports (Haycock and Haycock, 1991; Lindgren et al., 2002), our results showed an increase of TH activity rate by PKA-mediated Ser40 phosphorylation and by inhibition of protein phosphatases with Ok (Figs. 6–7). Despite this agrees with literature, we still observed modified time- and concentration-dependent decays of
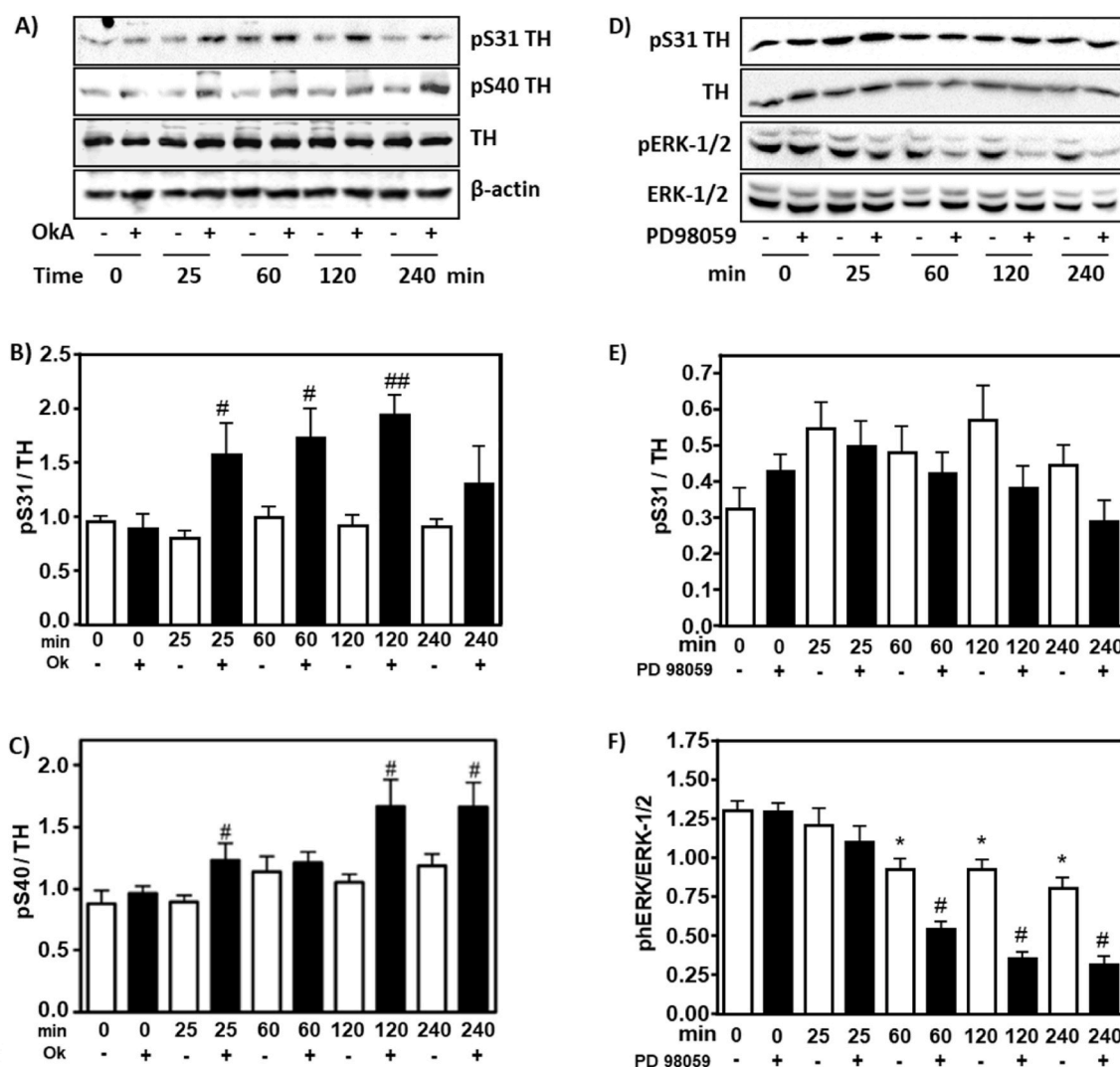
Fig. 7. TH phosphorylation changes in response to okadaic acid and to PD98059 at different times. A) TH phosphorylation at Ser31 and at Ser40 was determined by Western blot after different incubation times with or without 1 μM okadaic acid (Ok, added at time 0). In addition to total TH, β-actin (A) was also assessed as loading control. Mean optical density of the 55 kDa bands in A) were standardized to arbitrary units in each blot and results are expressed as pTH/TH ratio for Ser31 (B) and Ser40 (C). D) TH phosphorylation at Ser31 was determined with or without 25 μM PD98059 at different incubation times by Western blot. Dually phosphorylated ERK-1/2 in Thr202/Tyr204 was also determined as a control of PD98059 action. E) Results from D) are expressed as pS31 TH/TH ratio of standardized optical density of the 55 kDa bands. F) Graph showing phosphoERK/ERK-1/2 ratio of standardized optical density of the 42–44 kDa dimer from D). Data represent the means ± SEM of N equal to 4–5 brain striatal tissue incubations in all graphs. 0 min samples were not incubated. B–C) $^{\#}p < 0.05$, $^{\#\#}p < 0.01$ vs. 0 min incubation with Ok. F) $^{\#}p < 0.01$ vs. 0 min incubation without PD98059 (white bars); $^{*}p < 0.0001$ vs. 0 min incubation with PD98059 (black bars), ANOVA plus Sidak's multiple comparisons test.

[³H]-DA synthesis in brain tissue (Fig. 6) that are not apparently related to a loss of phosphorylation during the incubation (Figs. 7 and 8). Therefore, it is possible that binding of newly-formed DA to the TH low-affinity binding site/conformation may act as a physiological DA sensor (Dickson and Briggs, 2013; Gordon et al., 2008, 2009) indicating that synaptic vesicles are nearly filled in brain. Additionally, no changes in TH protein levels were observed during Ok treatment after 4 h (Figs. 7 and S3). This lack of effect agrees with results observed in PC12D cells, where the TH protein levels remains unaltered even after 24h of incubation with Ok (Kawahata et al., 2009).

TH phosphorylation in Ser31 is more frequent than Ser40 (Fig. 8 and Dunkley and Dickson, 2019). Ser31 is considered an ERK target site. We showed that ERK is active at the beginning of our incubation (Fig. 7F), and ERK pathway inhibition with PD98059 decreased TH activity (Fig. 6A). However, an incubation time-dependent decay of TH activity was observed even in the presence of PD98059 (Fig. 6A). Since Ser31-TH phosphorylation in brain does not seem to undergo major changes

during incubation (Figs. 7E and 8), the DA feedback on TH we observe also seems unrelated to Ser31- TH phosphorylation.

We found TH phosphorylation in Thr30 in rat brain by mass spectrometry (Fig. 8). To our knowledge this is a novel finding, of unknown physiological relevance. Thr30 is conserved in rat and mouse, but not in human TH sequences, while Ser31 and Ser40 are in all three species. Further work is necessary in this regard.

Our simple methodology can be replicated in many HPLC-equipped labs and become relevant to understand and refine treatments for DA-related disorders. The spontaneous endogenous DA accumulation allows to compare synaptic drug effects in fresh brain tissue without animal handing. A vesicular storage disorder may contribute to the etiopathogenesis of Parkinson's disease (Pifl et al., 2014). Accordingly, VMAT2 overexpression and L-DOPA raised DA storage. However, L-DOPA and TBZ treatments to human subjects should increase cytosolic DA (Fasano and Bentivoglio, 2009; Mosharov et al., 2009; Qi et al., 2008) as they increase DOPAC (Figs. 3 and 4). TBZ is FDA-approved for
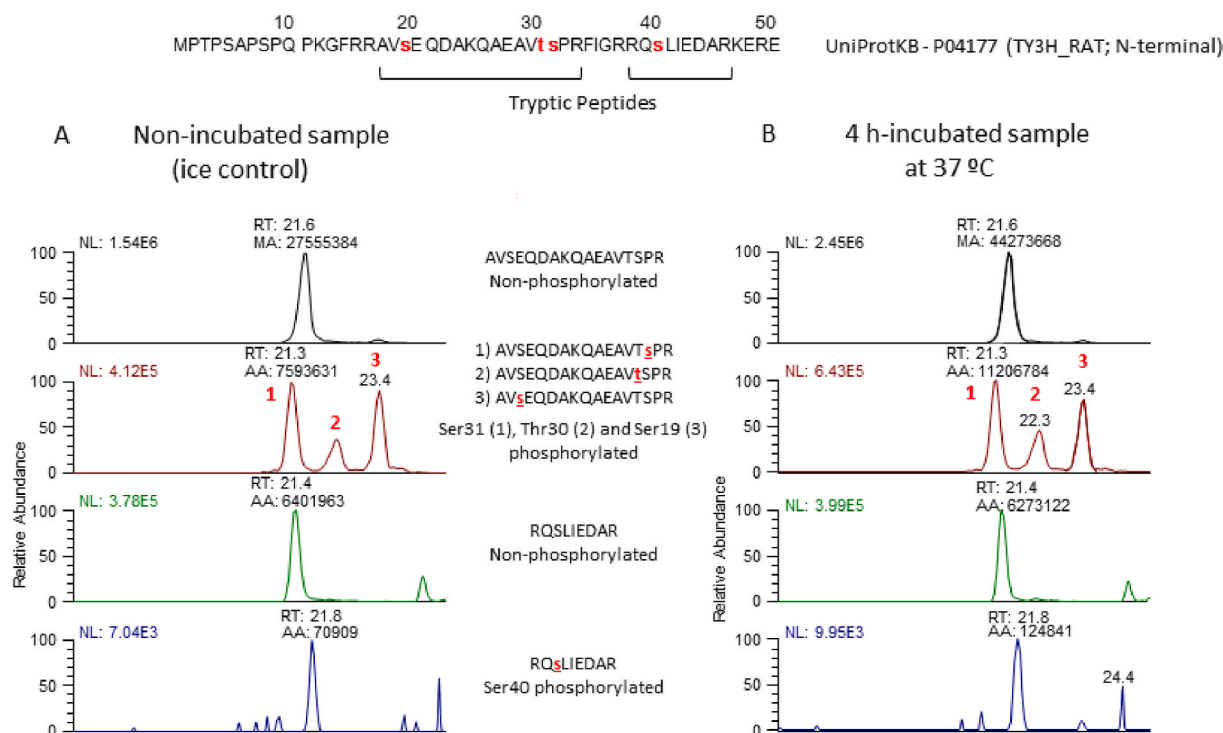
Fig. 8. LC-MS assessment of rat TH N-terminal phosphorylation in non-incubated (A) and 4h-incubated striatal samples (B). Top: UniProt rat TH sequence with tryptic peptides and phosphorylation sites (red) identified. Center: Rat TH peptide fragments identified by HPLC-MS after TH-immunoprecipitation and tryptic digestion. RT: retention time; NL: intensity; MA/AA: Manual or automatic peak area. s: phosphorylated serine; S: non-phosphorylated serine. Ratios of serine phosphorylation signals (s/S) were obtained from peak areas shown, which reflect peptide abundance and ionization efficiency. Threonine30 phosphorylation was observed (t, peak #2; T, non-phosphorylated threonine). The spectrometric analysis was performed in a data dependent mode, acquiring a full scan followed by 8 MS/MS scans of the 8 most intense signals from the inclusion list (see Supplementary Table S1).

Huntington's disease (Scott, 2011). VMAT2 inhibition by TBZ should increase cytosolic DA that produces a strong feedback on TH, which in turn could contribute to its antihyperkinetic benefits. VMAT2 and TH inhibition have been a target for the treatment of psychoses and addictions (Carlsson et al., 1972; Qi et al., 2008; Wimalasena, 2011): the non-selective VMAT inhibitor reserpine was used as antipsychotic. Of note, cytoplasmic DA accumulation can induce the formation of quinones and tetrahydroisoquinolines which have been involved in the degeneration of dopaminergic neurons (Goldstein et al., 2012) and interfere with DA synthesis (Scholz et al., 2008). Thus, it is worth considering the relevance of TH inhibition together with vesicular storage when understanding drug effects in these disorders. Mathematical models could be developed that consider TH inhibition as a factor to optimize drug doses and their combinations, together with experimental testing in brain *ex vivo* before animal and clinical research is carried out. Accordingly, understanding the inhibition of DA synthesis through TH feedback control offers real alternative possibilities for pharmacological intervention that could lead to new treatment strategies for DA-related disorders.

CRediT authorship contribution statement

Marta González-Sepúlveda: Conceptualization, Methodology, Formal analysis, Investigation, Writing, Visualization. **Muhammad Yusof Omar:** Investigation, Visualization. **Sally Hamdon:** Investigation. **Guofen Ma:** Investigation. **Santi Rosell-Vilar:** Methodology, Investigation. **Noora Raivio:** Validation, Investigation. **Doaa Abass:** Validation, Investigation. **Anna Martínez-Rivas:** Validation, Investigation. **Miquel Vila:** Methodology, Funding acquisition. **Jesús Giraldo:** Formal analysis, Funding acquisition. **Montserrat Carrascal:** Methodology, Investigation, Writing, Visualization. **Joaquín Abián:** Methodology, Writing, Funding acquisition. **Carles Gil:** Investigation, Writing,

Visualization. **Josefa Sabriá:** Conceptualization, Writing. **Jordi Ortiz:** Conceptualization, Methodology, Writing, Funding acquisition. **David Moreno-Delgado:** Conceptualization, Methodology, Formal analysis, Investigation.

Appendix A. Supplementary data

Supplementary data to this article can be found online at https://doi.org/10.1016/j.neuropharm.2022.109058.

References

Aghajanian, G.K., Roth, R.H., 1970. Gamma-hydroxybutyrate-induced increase in brain dopamine: localization by fluorescence microscopy. J. Pharmacol. Exp. Therapeut. 175, 131–138. https://jpet.aspetjournals.org/content/175/1/131.

Andén, N.E., Magnusson, T., Stock, G., 1973. Effects of drugs influencing monoamine mechanisms on the increase in brain dopamine produced by axotomy or treatment with gammahydroxybutyric acid. Naunyn-Schmiedeberg's Arch. Pharmacol. 278, 363–372. https://doi.org/10.1007/BF00501480.

Ankenman, R., Salvatore, M.F., 2007. Low dose alpha-methyl-para-tyrosine (AMPT) in the treatment of dystonia and dyskinesia. J. Neuropsychiatry Clin. Neurosci. 19, 65–69. https://doi.org/10.1176/jnp.2007.19.1.65.

Best, J.A., Nijhout, H.F., Reed, M.C., 2009. Homeostatic mechanisms in dopamine synthesis and release: a mathematical model. Theor. Biol. Med. Model. 6, 21. https://doi.org/10.1186/1742-4682-6-21.

Bolea, I., Colivicchi, M.A., Ballini, C., Marco-Contelles, J., Tipton, K.F., Unzeta, M., Della Corte, L., 2014. Neuroprotective effects of the MAO-B inhibitor, PF9601N, in an in vivo model of excitotoxicity. CNS Neurosci. Ther. 20, 641–650. https://doi.org/10.1111/cns.12271.

Briggs, G.D., Bulley, J., Dickson, P.W., 2014. Catalytic domain surface residues mediating catecholamine inhibition in tyrosine hydroxylase. J. Biochem. 155, 183–193. https://doi.org/10.1093/jb/mvt110.

Briggs, G.D., Gordon, S.L., Dickson, P.W., 2011. Mutational analysis of catecholamine binding in tyrosine hydroxylase. Biochemistry 50, 1545–1555. https://doi.org/10.1021/bi101455b.

Carballo-Carbajal, I., Laguna, A., Romero-Giménez, J., Cuadros, T., Bové, J., Martinez-Vicente, M., Parent, A., Gonzalez-Sepulveda, M., Peñuelas, N., Torra, A., Rodríguez-Galván, B., Ballabio, A., Hasegawa, T., Bortolozzi, A., Gelpi, E., Vila, M., 2019. Brain tyrosinase overexpression implicates age-dependent neuromelanin production in Parkinson's disease pathogenesis. Nat. Commun. 10 https://doi.org/10.1038/s41467-019-08858-y.

Carlsson, A., Persson, T., Roos, B.E., Wålinder, J., 1972. Potentiation of phenothiazines by α-methyltyrosine in treatment of chronic schizophrenia. J. Neural. Transm. 33, 83–90. https://doi.org/10.1007/BF01260898.

Casanovas, A., Carrascal, M., Abián, J., López-Tejero, M.D., Llobera, M., 2009. Discovery of lipoprotein lipase pI isoforms and contributions to their characterization. J. Proteonomics 72, 1031–1039. https://doi.org/10.1016/j.jprot.2009.06.002.

Daubner, S.C., Le, T., Wang, S., 2011. Tyrosine hydroxylase and regulation of dopamine synthesis. Arch. Biochem. Biophys. 508, 1–12. https://doi.org/10.1016/j.abb.2010.12.017.

Dickson, P.W., Briggs, G.D., 2013. In: Tyrosine Hydroxylase. Regulation by Feedback Inhibition and Phosphorylation, first ed. Elsevier Inc. https://doi.org/10.1016/B978-0-12-411512-5.00002-6. Advances in Pharmacology.

Dunkley, P.R., Bobrovskaya, L., Graham, M.E., Von Nagy-Felsobuki, E.I., Dickson, P.W., 2004. Tyrosine hydroxylase phosphorylation: regulation and consequences. J. Neurochem. 91, 1025–1043. https://doi.org/10.1111/j.1471-4159.2004.02797.x.

Dunkley, P.R., Dickson, P.W., 2019. Tyrosine hydroxylase phosphorylation in vivo. J. Neurochem. 149, 706–728. https://doi.org/10.1111/jnc.14675.

Eisenhofer, G., Kopin, I.J., Goldstein, D.S., 2004. Leaky catecholamine stores: undue waste or a stress response coping mechanism? Ann. N. Y. Acad. Sci. 1018, 224–230. https://doi.org/10.1196/annals.1296.027.

Fasano, A., Bentivoglio, A.R., 2009. Tetrabenazine. Expert Opin. Pharmacother. 10, 2883–2896. https://doi.org/10.1517/14656560903386292.

Ghorbani, S., Szigetvari, P.D., Haavik, J., Kleppe, R., 2020. Serine 19 phosphorylation and 14-3-3 binding regulate phosphorylation and dephosphorylation of tyrosine hydroxylase on serine 31 and serine 40. J. Neurochem. 152, 29–47. https://doi.org/10.1111/JNC.14872.

Goldstein, D.S., Sullivan, P., Cooney, A., Jinsmaa, Y., Sullivan, R., Gross, D.J., Holmes, C., Kopin, I.J., Sharabi, Y., 2012. Vesicular uptake blockade generates the toxic dopamine metabolite 3,4-dihydroxyphenylacetaldehyde in PC12 cells: relevance to the pathogenesis of Parkinson's disease. J. Neurochem. 123, 932–943. https://doi.org/10.1111/j.1471-4159.2012.07924.x.

Gordon, S.L., Quinsey, N.S., Dunkley, P.R., Dickson, P.W., 2008. Tyrosine hydroxylase activity is regulated by two distinct dopamine-binding sites. J. Neurochem. 106, 1614–1623. https://doi.org/10.1111/j.1471-4159.2008.05509.x.

Gordon, S.L., Webb, J.K., Shehadeh, J., Dunkley, P.R., Dickson, P.W., 2009. The low affinity dopamine binding site on tyrosine hydroxylase: the role of the N-terminus and in situ regulation of enzyme activity. Neurochem. Res. 34, 1830–1837. https://doi.org/10.1007/s11064-009-9989-5.

Gu, C., Ewing, A.G., 2021. Simultaneous detection of vesicular content and exocytotic release with two electrodes in and at a single cell. Chem. Sci. 12, 7393–7400. https://doi.org/10.1039/D1SC01190A.

Harada, K., Wu, J., Haycock, J.W., Goldstein, M., 1996. Regulation of L-DOPA biosynthesis by site-specific phosphorylation of tyrosine hydroxylase in AtT-20 cells expressing wild-type and serine 40-substituted enzyme. J. Neurochem. 67, 629–635. https://onlinelibrary.wiley.com/doi/full/10.1046/j.1471-4159.1996.67020629.x.

Haycock, J.W., Haycock, D.A., 1991. Tyrosine hydroxylase in rat brain dopaminergic nerve terminals. Multiple-site phosphorylation in vivo and in synaptosomes. J. Biol. Chem. 266, 5650–5657. https://linkinghub.elsevier.com/retrieve/pii/S0021-9258(19)67644-1.

Jankovic, J., 2016. Dopamine depleters in the treatment of hyperkinetic movement disorders, Expert Opinion on Pharmacotherapy. Taylor & Francis. https://doi.org/10.1080/14656566.2016.1258063.

Justice, J.B., Nicolaysen, L.C., Michael, A.C., 1988. Modeling the dopaminergic nerve terminal. J. Neurosci. Methods 22, 239–252. https://doi.org/10.1016/0165-0270(88)90045-3.

Kawahata, I., Tokuoka, H., Parvez, H., Ichinose, H., 2009. Accumulation of phosphorylated tyrosine hydroxylase into insoluble protein aggregates by inhibition of an ubiquitin-proteasome system in PC12D cells. J. Neural. Transm. 116, 1571–1578. https://doi.org/10.1007/S00702-009-0304-Z.

Lindgren, N., Goiny, M., Herrera-Marschitz, M., Haycock, J.W., Hökfelt, T., Fisone, G., Hokfelt, T., Fisone, G., 2002. Activation of extracellular signal-regulated kinases 1 and 2 by depolarization stimulates tyrosine hydroxylase phosphorylation and dopamine synthesis in rat brain. Eur. J. Neurosci. 15, 769–773. https://doi.org/10.1046/j.1460-9568.2002.01901.x.

Lindgren, N., Xu, Z.Q.D., Lindskog, M., Herrera-Marschitz, M., Goiny, M., Haycock, J., Goldstein, M., Hökfelt, T., Fisone, G., 2000. Regulation of tyrosine hydroxylase activity and phosphorylation at Ser19 and Ser40 via activation of glutamate NMDA receptors in rat striatum. J. Neurochem. 74, 2470–2477. https://doi.org/10.1046/j.1471-4159.2000.0742470.x.

Ludders, J.W., 1992. Advantages and guidelines for using isoflurane. In: Veterinary Clinics of North America - Small Animal Practice, pp. 328–331. https://doi.org/10.1016/S0195-5616(92)50626-X.

Ma, G.F., Raivio, N., Sabrià, J., Ortiz, J., 2014. Agonist and antagonist effects of aripiprazole on D2-like receptors controlling rat brain dopamine synthesis depend on the dopaminergic tone. Int. J. Neuropsychopharmacol. pyu046 https://doi.org/10.1093/ijnp/pyu046.

McCulloch, R.I., Daubner, S.C., Fitzpatrick, P.F., 2001. Effects of substitution at serine 40 of tyrosine hydroxylase on catecholamine binding. Biochemistry 40, 7273–7278. https://doi.org/10.1021/bi010546d.

Mor, D.E., Tsika, E., Mazzulli, J.R., Gould, N.S., Kim, H., Daniels, M.J., Doshi, S., Gupta, P., Grossman, J.L., Tan, V.X., Kalb, R.G., Caldwell, K.A., Caldwell, G.A., Wolfe, J.H., Ischiropoulos, H., 2017. Dopamine induces soluble α-synuclein oligomers and nigrostriatal degeneration. Nat. Neurosci. 20, 1560–1568. https://doi.org/10.1038/nn.4641.

Mosharov, E.V., Larsen, K.E., Kanter, E., Phillips, K.A., Wilson, K., Schmitz, Y., Krantz, D. E., Kobayashi, K., Edwards, R.H., Sulzer, D., 2009. Interplay between cytosolic dopamine, calcium, and alpha-synuclein causes selective death of substantia nigra neurons. Neuron 62, 218–229. https://doi.org/10.1016/j.neuron.2009.01.033.

Mosharov, E.V., Staal, R.G.W., Bové, J., Prou, D., Hananiya, A., Markov, D., Poulsen, N., Larsen, K.E., Moore, C.M.H., Troyer, M.D., Edwards, R.H., Przedborski, S., Sulzer, D., 2006. Alpha-synuclein overexpression increases cytosolic catecholamine concentration. J. Neurosci. 26, 9304–9311. https://doi.org/10.1523/JNEUROSCI.0519-06.2006.

Nakashima, A., Hayashi, N., Kaneko, Y.S., Mori, K., Sabban, E.L., Nagatsu, T., Ota, A., 2009. Role of N-terminus of tyrosine hydroxylase in the biosynthesis of catecholamines. J. Neural. Transm. 116, 1355–1362. https://doi.org/10.1007/s00702-009-0227-8.

Nakashima, A., Kaneko, Y.S., Kodani, Y., Mori, K., Nagasaki, H., Nagatsu, T., Ota, A., 2013. Intracellular stability of tyrosine hydroxylase: phosphorylation and proteasomal digestion of the enzyme. Adv. Pharmacol. 68, 3–11. https://doi.org/10.1016/B978-0-12-411512-5.00001-4.

Ortiz, J., Gómez, J., Torrent, A., Aldavert, M., Blanco, I., 2000. Quantitative radioisotopic determination of histidine decarboxylase using high-performance liquid chromatography. Anal. Biochem. 280, 111–117. https://doi.org/10.1006/abio.2000.4494.

Paxinos, G., Watson, C., 1982. The Rat Brain in Stereotaxic Coordinates. Acad. Press. United States Am.

Pifl, C., Rajput, A.H.A., Reither, H., Blesa, J., Cavada, C., Obeso, J.A., Rajput, A.H.A., Hornykiewicz, O., 2014. Is Parkinson's disease a vesicular dopamine storage disorder? Evidence from a study in isolated synaptic vesicles of human and nonhuman primate striatum. J. Neurosci. 34, 8210–8218. https://doi.org/10.1523/JNEUROSCI.5456-13.2014.

Qi, Zhen, Miller, G.W., Voit, E.O., 2008. Computational systems analysis of dopamine metabolism. PLoS One 3, e2444. https://doi.org/10.1371/journal.pone.0002444.

Qi, Z., Miller, G.W., Voit, E.O., 2008. A mathematical model of presynaptic dopamine homeostasis: implications for schizophrenia. Pharmacopsychiatry 41 (Suppl. 1), S89–S98. https://doi.org/10.1055/s-2008-1080936.

Ramsey, A.J., Fitzpatrick, P.F., 1998. Effects of phosphorylation of serine 40 of tyrosine hydroxylase on binding of catecholamnines: evidence for a novel regulatory mechanism. Biochemsitry 37, 8980–8986. https://doi.org/10.1021/bi980582l.

Scholz, J., Toska, K., Luborzewski, A., Maass, A., Schünemann, V., Haavik, J., Moser, A., 2008. Endogenous tetrahydroisoquinolines associated with Parkinson's disease mimic the feedback inhibition of tyrosine hydroxylase by catecholamines. FEBS J. 275, 2109–2121. https://doi.org/10.1111/j.1742-4658.2008.06365.x.

Scott, L.J., 2011. Tetrabenazine: for chorea associated with Huntington's disease. CNS Drugs 25, 1073–1085. https://doi.org/10.2165/11208330-000000000-00000.

Spector, S., Gordon, R., Sjoerdsma, A., Udenfriend, S., 1967. End-product inhibition of tyrosine hydroxylase as a possible mechanism for regulation of norepinephrine synthesis. Mol. Pharmacol. 3, 549–555. http://molpharm.aspetjournals.org/cgi/pmidlookup?view=long&pmid=6075244.

Sura, G.R., Daubner, S.C., Fitzpatrick, P.F., 2004. Effects of phosphorylation by protein kinase A on binding of catecholamines to the human tyrosine hydroxylase isoforms. J. Neurochem. 90, 970–978. https://doi.org/10.1111/j.1471-4159.2004.02566.x.

Tekin, I., Roskoski, R., Carkaci-Salli, N., Vrana, K.E., 2014. Complex molecular regulation of tyrosine hydroxylase. J. Neural. Transm. https://doi.org/10.1007/s00702-014-1238-7.

Wallace, L.J., 2007. A small dopamine permeability of storage vesicle membranes and end product inhibition of tyrosine hydroxylase are sufficient to explain changes occurring in dopamine synthesis and storage after inhibition of neuron firing. Synapse 61, 715–723. https://doi.org/10.1002/syn.20408.

Walters, J.R., Roth, R.H., Aghajanian, G.K., 1973. Dopaminergic neurons: similar biochemical and histochemical effects of gamma-hydroxybutyrate and acute lesions of the nigro-neostriatal pathway. J. Pharmacol. Exp. Therapeut. 186, 630–639. https://jpet.aspetjournals.org/content/186/3/630.

Wimalasena, K., 2011. Vesicular monoamine transporters: structure-function, pharmacology, and medicinal chemistry. Med. Res. Rev. 31, 483–519. https://doi.org/10.1002/med.20187.

Zhang, S., Huang, T., Ilangovan, U., Hinck, A.P., Fitzpatrick, P.F., 2014. The solution structure of the regulatory domain of tyrosine hydroxylase. J. Mol. Biol. 426, 1483–1497. https://doi.org/10.1016/j.jmb.2013.12.015.